J. Phys.: Condens. Matter **22** (2010) 334220 (7pp) doi:10.1088/0953-8984/22/33/334220

Designing rigid carbon foams

Sora Park[1], Kritsada Kittimanapun[2], Jeung Sun Ahn[1], Young-Kyun Kwon[1] and David Tománek[1,2]

[1] Department of Physics and Research Institute for Basic Sciences, Kyung Hee University, Seoul, 130-701, Korea
[2] Physics and Astronomy Department, Michigan State University, East Lansing, MI 48824-2320, USA

E-mail: ykkwon@khu.ac.kr and tomanek@pa.msu.edu

Received 24 November 2009
Published 4 August 2010
Online at stacks.iop.org/JPhysCM/22/334220

Abstract
We use *ab initio* density functional calculations to study the stability, elastic properties and electronic structure of sp^2 carbon minimal surfaces with negative Gaussian curvature, called schwarzites. We focus on two systems with cubic unit cells containing 152 and 200 carbon atoms, which are metallic and very rigid. The porous schwarzite structure allows for efficient and reversible doping by electron donors and acceptors, making it a promising candidate for the next generation of alkali ion batteries. We identify schwarzite structures that act as arrays of interconnected spin quantum dots or become magnetic when doped. We introduce two interpenetrating schwarzite structures that may find their use as the ultimate super-capacitor.

(Some figures in this article are in colour only in the electronic version)

1. Introduction

Nanostructured carbon has become an intensely researched topic since the discovery of the C_{60} molecule [1], a previously unknown carbon allotrope. Most research has focused on structures with zero or positive Gaussian curvature such as fullerenes, nanotubes and graphene [2, 3]. Much less emphasis has been placed on structures with negative Gaussian curvature [4–18], related to foams, which may be equally rigid and exhibit unusual electronic and magnetic properties. These systems, also called schwarzites, are space-filling contiguous structures formed of sp^2 bonded carbon. They are unique in their ability to subdivide space into two disjoint, contiguous subspaces with labyrinthine morphology and the same infinite spatial extent.

Here we focus on two schwarzite structures with cubic unit cells containing between 152 and 200 carbon atoms. We also postulate a structure with 400 atoms per unit cell as a representative of a class of interpenetrating, but disconnected schwarzite lattices. Using *ab initio* density functional calculations, we determine the equilibrium structure as well as the elastic, electronic and magnetic properties of pristine and electron or hole doped schwarzites. Our calculations indicate the possibility of tuning the concentration of K and Cl atoms in order to achieve magnetic behavior. We find that the hole doped C_{200} structure and similar systems may behave as an array of interconnected spin quantum dots. We discuss potential energy storage applications of schwarzites, such as next-generation electrodes for alkali ion batteries, and calculate the capacitance of two interpenetrating schwarzites, which may find their use as the ultimate super-capacitor.

2. Computational method

Our *ab initio* calculations are based on the density functional theory (DFT) within the local density approximation (LDA) and use the Ceperley–Alder exchange–correlation functional [19] as parameterized by Perdew and Zunger [20]. Interactions between valence electrons and ions are treated by norm-conserving pseudopotentials [21] with separable non-local operators [22]. Atomic orbitals with double-ζ polarization are used to expand the electron wavefunctions [23, 24] with an energy cutoff of 210 Ryd for the real-space mesh. We use 0.02 Ryd as the confinement energy shift that defines the cutoff radii of the atomic orbitals. We sample the small Brillouin zone by 8 k-points in order to represent the Bloch wavefunctions for the momentum-space integration. All geometries are optimized using the conjugate gradient method [25], until none of the residual Hellmann–Feynman forces acting on any atom exceeds 1.56×10^{-3} Ryd/a_B, where a_B is the Bohr radius.

 © 2010 IOP Publishing Ltd Printed in the UK & the USA

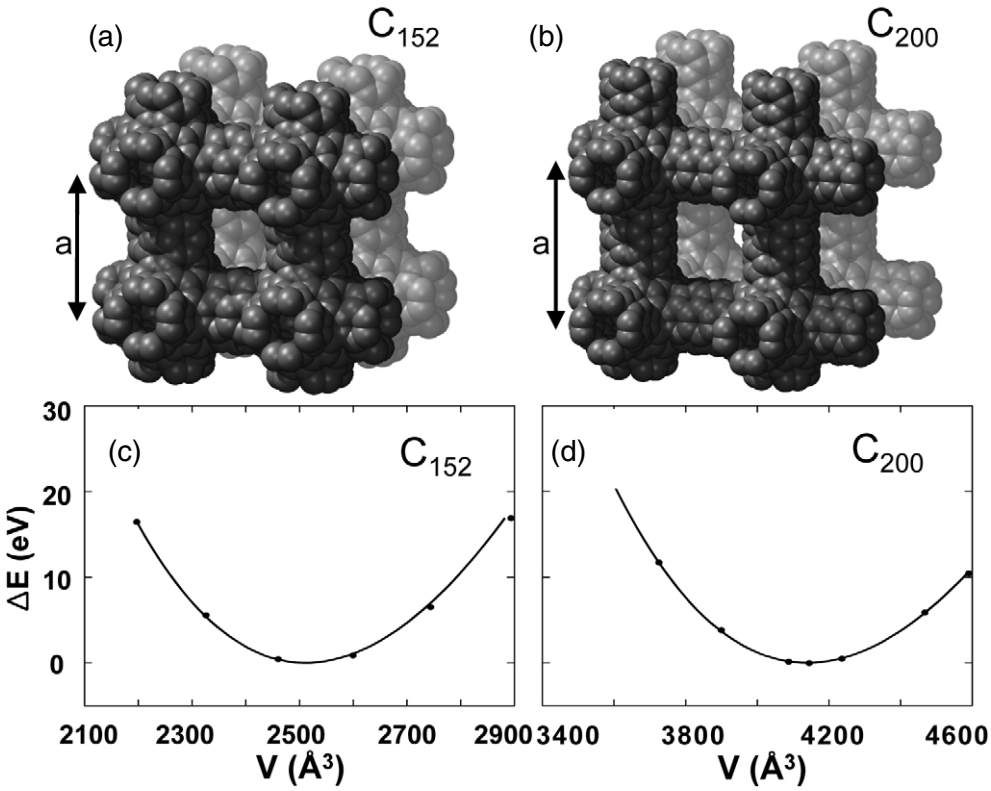

Figure 1. Equilibrium geometry of P schwarzites with 152 (a) and 200 (b) carbon atoms per cubic unit cell with lattice constant a and volume $V = a^3$. Total energy change ΔE as a function of V for the C_{152} (c) and C_{200} (d) schwarzites.

3. Results

3.1. Pristine schwarzite lattices

Previous theoretical studies addressed schwarzites with 24 [9], 32 [10], 48 [11], 56 [11, 12], 72 [12], 80 [12], 168 [13, 15], 192 [14, 15], 200 [11], 216 [15, 16], and 224 [17] atoms per unit cell, or related general morphology issues [17, 18]. We focus on two structures with a primitive (P) minimal surface spanned by an underlying simple cubic lattice, which have not been studied previously and which contain 152 and 200 carbon atoms per unit cell. The C_{152} structure is depicted in figure 1(a) and the C_{200} structure in figure 1(b). The unit cells of either schwarzite contain one 'core' structure with O_h symmetry and a negative local Gaussian curvature. The six extremities of the cores are connected to neighboring cores by (4, 4) carbon nanotube segments of various length to form a contiguous lattice. Negative Gaussian curvature is introduced by the presence of heptagons in the graphitic lattice. Our systems contain exactly 24 heptagons per unit cell in accordance with Euler's theorem. The heptagons along with 24 hexagons, form the cores of the schwarzite. Each interconnect contains one nanotube unit cell with 8 hexagons in the C_{152} structure and two unit cells with 16 hexagons in the C_{200} structure.

To identify the equilibrium structure and elastic properties of the two schwarzite structures, we performed a series of structure optimizations at fixed unit cell volume. The total energy change $\Delta E(V)$ with respect to the optimum structure is presented for the two structures in figures 1(c) and (d) along with Murnaghan function fits of our data. For the C_{152} schwarzite we find the binding energy $E_{coh} = 10.50$ eV/atom at the equilibrium volume $V_{eq} = 2515$ Å^3, corresponding to the lattice constant $a = 13.60$ Å, gravimetric density $\rho = 1.21$ g cm^{-3} and bulk modulus $B = 111$ GPa. The less dense C_{200} schwarzite structure is slightly more stable with $E_{coh} = 10.52$ eV/atom at $V_{eq} = 4141$ Å^3, corresponding to $a = 16.06$ Å, but has a smaller gravimetric density $\rho = 0.96$ g cm^{-3} and bulk modulus $B = 76.4$ GPa. The reduction of the binding energy with respect to the value of 10.88 eV/atom in a graphene monolayer is caused by the strain associated with curvature and is similar in value to carbon nanotubes. We find both structures to be substantially lighter than graphite ($\rho = 2.27$ g cm^{-3}) and diamond [26] ($\rho = 3.54$ g cm^{-3}). Also the bulk modulus of the stiffer C_{152} is about four times smaller than the diamond value [26] $B_{expt} = 442$ GPa.

To characterize the electronic properties of these schwarzites, we calculated their electronic density of states and band structure. The electronic densities of states of C_{152} and C_{200}, presented in figures 2(a) and (b), indicate that both structures are metallic. The origin of the individual peaks in the density of states can be traced back to the band structure graphs in figures 2(c) and (d). The schwarzites exhibit narrow band gaps above and, in the case of C_{200}, also below the Fermi level. Furthermore, as seen in figures 2(b) and (d), the C_{200} structure exhibits a 3-fold degenerate flat band about 0.62 eV below the Fermi level. Since in neither structure the Fermi level falls into a sharp peak, both structures are non-magnetic.

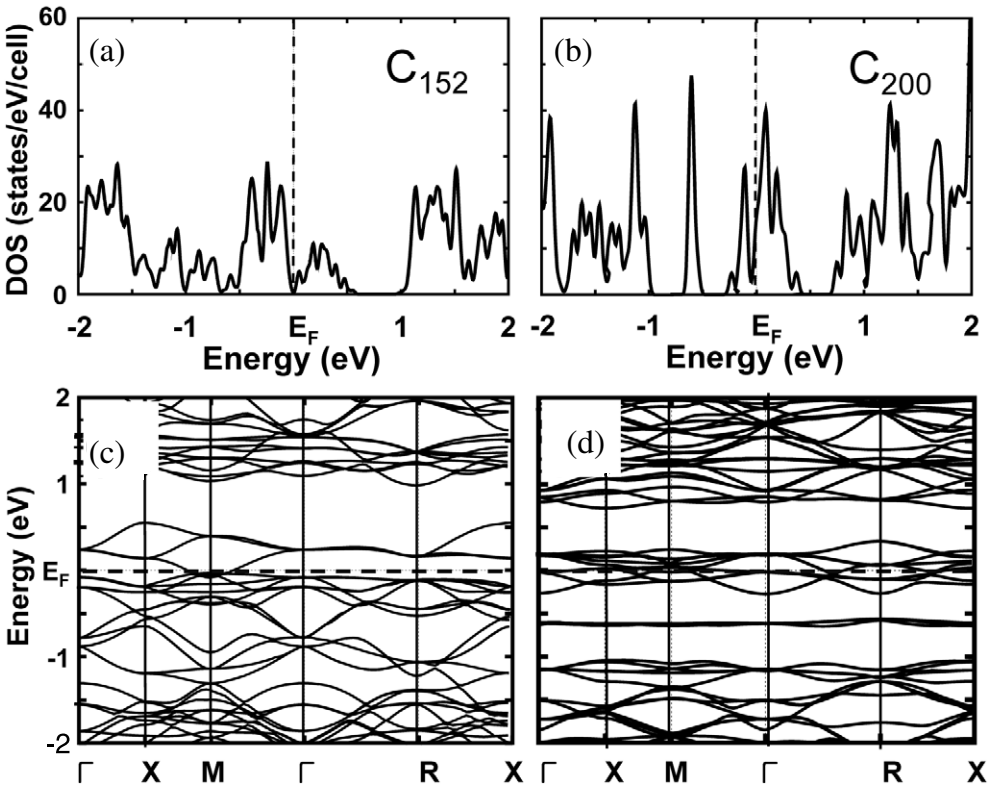

Figure 2. Electronic structure of schwarzites. Density of states of the optimized schwarzite structures with unit cells containing 152 (a) and 200 (b) C atoms, smoothed by a Gaussian with the full width at half maximum of 0.03 eV. Corresponding band structure of the C_{152} (c) and C_{200} (d) schwarzites.

Besides the nonzero value of the density of states at E_F in the schwarzites we studied, which makes them metallic, the nature of states near the Fermi level is also very important for the dielectric response of the system. Therefore, we plot the electron density associated with the frontier states at the Fermi level of C_{152} in figure 3(a) and that of C_{200} in figure 3(b). We find the frontier states to be highly delocalized in both systems. In the larger C_{200} schwarzite, we note that the frontier states have a node in the middle of the tubular interconnects between the cores, indicated by an arrow in figure 3(b). As seen in figure 3(c), which depicts the electron density of C_{152} associated with the ≈0.8 eV wide band mostly below the Fermi level, the corresponding states are distributed nearly uniformly across the structure. To understand the origin of the flat band in the C_{200} schwarzite 0.62 eV below the Fermi level, we present the associated electron density in figure 3(d). We may characterize this state as an array of non-interacting quantum dots centered in the negative Gaussian curvature regions at the cores of the C_{200} structure. We expect such a state also to occur in other schwarzite structures of the same type, which have larger unit cells due to longer tubular interconnects.

3.2. Interpenetrating schwarzite lattices

The open space in the C_{152} and C_{200} structures, depicted in figures 1(a) and (b), can be filled by other atoms as external dopants. As we show in the following, and depict in figures 4(a) and (b), the open space in the C_{200} schwarzite is wide enough and ideally suited to accommodate even an identical replica of the C_{200} schwarzite in an unstrained lattice.

In either schwarzite described in this manuscript, the tubular interconnects are composed of (4, 4) carbon nanotubes. As seen in figures 4(a) and (b), the closest approach distance between the sublattices occurs in the geometry depicted in the inset of figure 4(c), with two (4, 4) nanotube segments standing normal to each other. To estimate the optimum inter-wall separation, we calculated the inter-tube interaction in this geometry and plotted the data points along with a Morse function fit in figure 4(c). We found the optimum inter-tube distance to be $d_{eq} = 7.8$ Å, corresponding to the closest inter-wall distance of 2.4 Å, somewhat smaller than the interlayer distance in graphite. The corresponding distance between adjacent tubular interconnects of the C_{200} substructures in C_{400}, as depicted in figures 4(a) and (b), is $d = 8.00$ Å, which indeed is very close to the optimum inter-tube distance value $d_{eq} = 7.8$ Å. Since the C_{400} schwarzite is structurally a superposition of two C_{200} schwarzite lattices, its gravimetric density is twice that of C_{200}, namely $\rho = 1.92$ g cm^{-3}. Also the bulk modulus of C_{400}, $B = 153$ GPa, is twice that of C_{200}, which is about one third of the diamond value.

As for the electronic density of states of the C_{200} sublattices, also that of the C_{400} schwarzite, shown in figure 4(d), has a large density of states at the Fermi level, indicating a metallic system. Similar to C_{200}, also C_{400} has a narrow band about 0.6 eV below E_F, associated with a lattice of very weakly coupled quantum dots. Careful comparison of

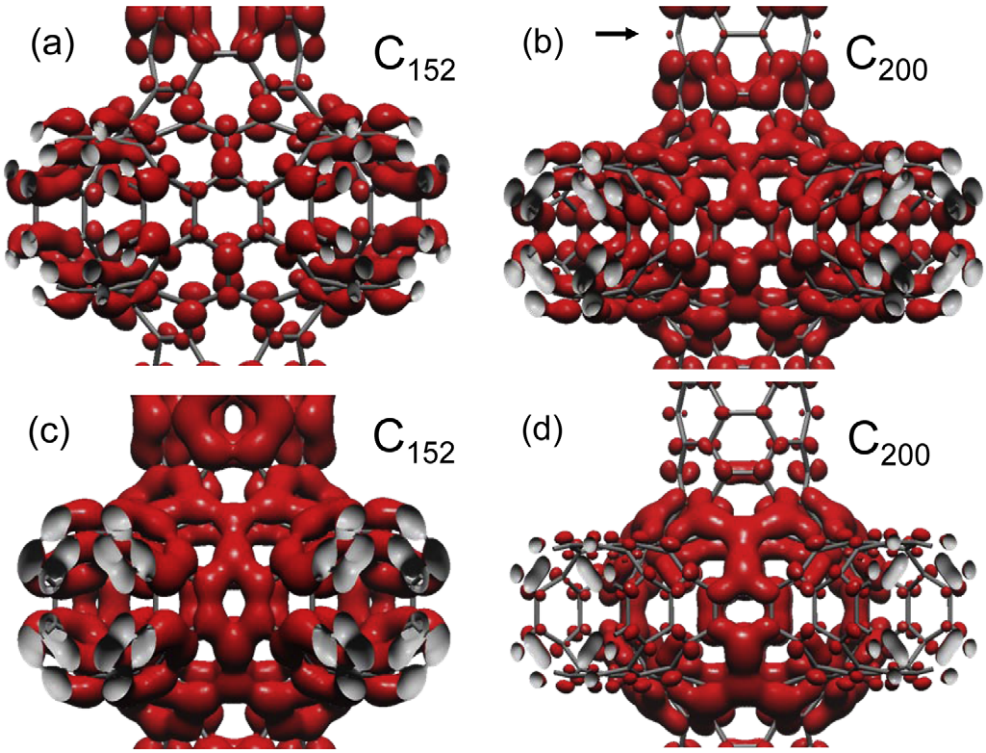

Figure 3. Electron densities in schwarzite structures containing 152 and 200 atoms per unit cell, presented as isodensity surfaces. Electron density associated with frontier states of C_{152} (a) and C_{200} (b) in the energy range $E_F - 0.15$ eV $< E < E_F + 0.15$ eV, presented at the isodensity value of 10^{-2} Å^{-3}. (c) Electron density of C_{152} associated with states in the energy range $E_F - 0.72$ eV $< E < E_F + 0.10$ eV, presented at the isodensity value of 10^{-2} Å^{-3}. (d) Electron density of C_{200} associated with the localized state near $E_F - 0.62$ eV, presented at the isodensity value of 10^{-4} Å^{-3}.

figures 2(b) and 4(d) indicates that the central band around E_F becomes wider in the C_{400} lattice in comparison to the C_{200} lattice. This band broadening is accompanied by a corresponding narrowing of the band gaps above and below this central band.

3.3. Intercalated schwarzites

As mentioned above, the empty space delimited by the schwarzite minimal surface can accommodate intercalant ions in order to shift the Fermi level. We consider K as a model donor that has been used widely in graphite intercalations compounds (GICs) [27]. Due to its highest electronic affinity in the periodic table [26] of 3.61 eV, we choose Cl as a model acceptor.

As in section 3.2, we focus on the C_{200} schwarzite structure. To maximize charge transfer between the intercalant atoms and the schwarzite lattice, we place one K or Cl atom in the center of each core of the schwarzite. To estimate the charge transfer between the intercalants and the schwarzite, we performed a Mulliken population analysis and, alternatively, integrated the total electron density within a sphere surrounding the intercalant ion. We found the Mulliken charge on K to be $+0.96e$ and that on Cl to be $-0.42e$. Electron density integration around the intercalant within schwarzite only makes sense up to the size of the cavity inside the core structure. Considering a sphere with a radius of $R = 2.4$ Å around Cl yields 7.00 valence electrons in the case of an isolated atom and 7.42 valence electrons in the case of Cl@C_{200}. Since the atomic radius of K is much larger, an isolated atom contains only 0.56 valence electrons within a sphere with $R = 2.4$ Å. Upon intercalation, in K@C_{200}, it loses almost all of the valence charge, so that only 0.01 valence electrons remain within this sphere.

By subtracting the total energy of C_{200} and the isolated atom A from that of A@C_{200}, where A = K or Cl, we found that the K atom stabilizes the unit cell by 2.080 eV, whereas the Cl atom provides a smaller stabilization by 0.636 eV per unit cell, partly due to the smaller charge transfer.

The ability to efficiently transfer most of the valence charge from the alkali atom to the graphitic structure is currently used in Li ion batteries, where Li is intercalated in between graphene layers in graphite, causing an ≈30% expansion in the direction normal to the graphene layers. Repeated expansion and contraction during charge/discharge cycles is known to reduce the lifetime of alkali ion batteries, as it causes structural rearrangement of the grains and eventually blocks diffusion pathways. No such adverse effects should occur in the rigid, but still conductive schwarzite structures, which may yield a new generation of advanced alkali ion batteries. As a different potential application of doped schwarzites, we wish to mention their potential for hydrogen storage, similar to Ca doped C_{60} crystals that proved to store reversibly molecular hydrogen [28] up to 8.4 wt%.

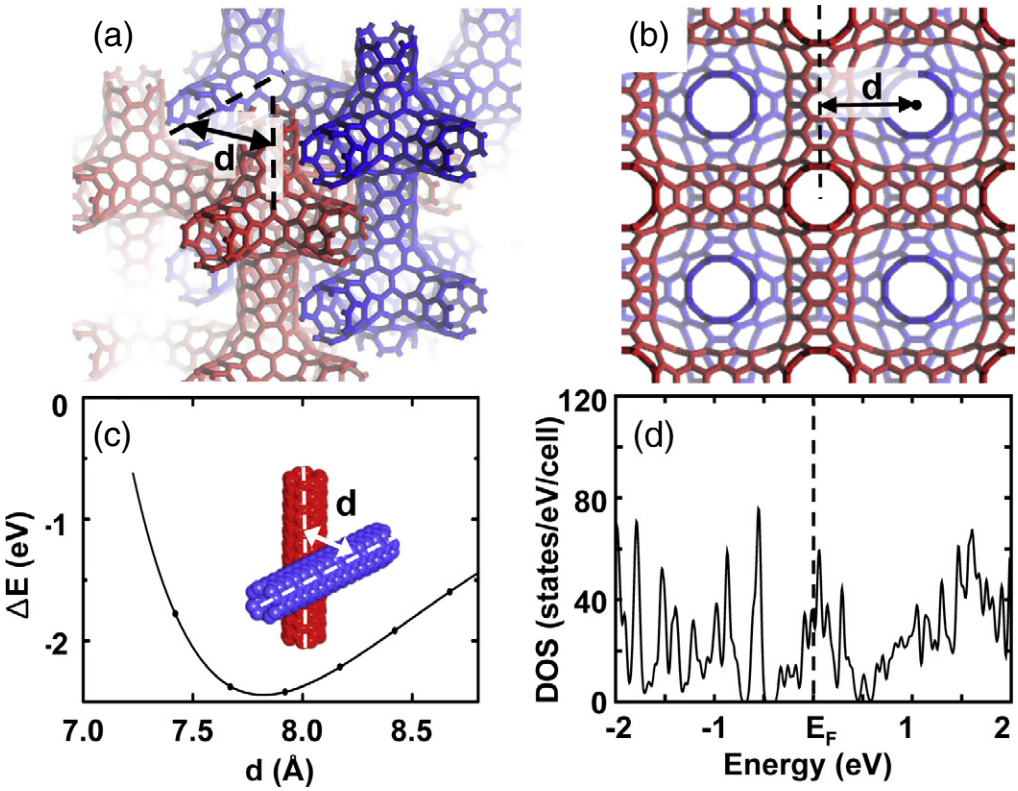

Figure 4. Equilibrium structure of two interpenetrating C_{200} schwarzite lattices, shown in figure 1(b), with 400 C atoms in total per unit cell, shown in perspective (a) and top (b) view. (c) Interaction energy between two (4, 4) nanotubes, with the geometry shown in the inset, representing the interaction between the tubular interconnects in the two interpenetrating C_{200} schwarzites. (d) Electronic density of states of the C_{400} schwarzite.

As suggested by the smaller amount of charge transferred from the C_{200} schwarzite to Cl ions, the effect of acceptor intercalation is much smaller than that of donor intercalation. Nevertheless, hole doping should make it possible to shift E_F down. Especially interesting appears the possibility to move the Fermi level into the region of the threefold degenerate flat band. Partial occupation of the band is expected to change the system to a ferromagnet with a magnetic moment per unit cell up to 6 μ_B. To determine the necessary amount of doping, we estimated the occupied portion of the band near E_F to carry 6 electrons. Combining this with the fact that the flat band also contains 6 electrons, we conclude that hole doping C_{200} with 7–11 electrons per unit cell should, assuming that the rigid band model applies, move the Fermi level into the region of the flat band. Using the charge transfer estimated for one Cl atom in C_{200}, this could be achieved by intercalating between ≈10–30 Cl atoms per unit cell. Using interatomic distances from free Cl_2, we believe that in the optimum case, Cl_6 clusters could be accommodated in the cores. Assuming that also each tubular interconnect could accommodate up to two Cl atoms, the Cl doped system should barely reach the criterion of partly depleting the initially flat band by Cl doping, causing ferromagnetism to occur.

To get an impression of how uniformly the transferred charge is distributed across the schwarzite lattice, we plot in figure 5(a) the distribution of the excess electron density in K@C_{200} and in figure 5(b) the corresponding distribution of the deficient electron density in Cl@C_{200}. Since both ions are well separated from the schwarzite lattice, we find that the transferred charge is distributed rather uniformly across the schwarzite in both cases.

Also the two interpenetrating C_{200} lattices, forming the C_{400} schwarzites, can be differentially doped, one with K and the other with Cl atoms, giving a net positive charge to one and a net negative charge to the other sublattice, similar to a capacitor. We superposed the K@C_{200} and Cl@C_{200} lattices and found a net stabilization with respect to separated K@C_{200} and Cl@C_{200} doped schwarzites of −15.735 eV. Similar to the doped sublattices, the Mulliken population analysis indicates that the net charge on K is close to $+0.70e$ and that on Cl is close to $-0.42e$. The opposite charges are then accommodated in the adjacent C_{200} substructure.

In the following we will estimate the capacitance of the schwarzite structure per 1 cm^3 volume. The capacitance of a parallel-plate capacitor of area A and inter-plate distance d, defining the volume $V = Ad$, is given by $C = \epsilon_0 A/d$ in SI units. For the sake of reference, an idealized capacitor with $V = 1$ cm^3, formed by a graphene bilayer with $d = 0.335$ nm, would have an area $A = 3.0 \times 10^3$ m^2 and a capacitance of 79.3 F. In the unit cell of the C_{400} schwarzite with the volume $V = 4.141$ nm^3, 200 carbon atoms are associated with one electrode. With an estimated area per carbon atom of 2.62 $Å^2$, the same as in graphene, we estimate that the area of one electrode per cm^3 schwarzite should be 1.3×10^3 m^2.

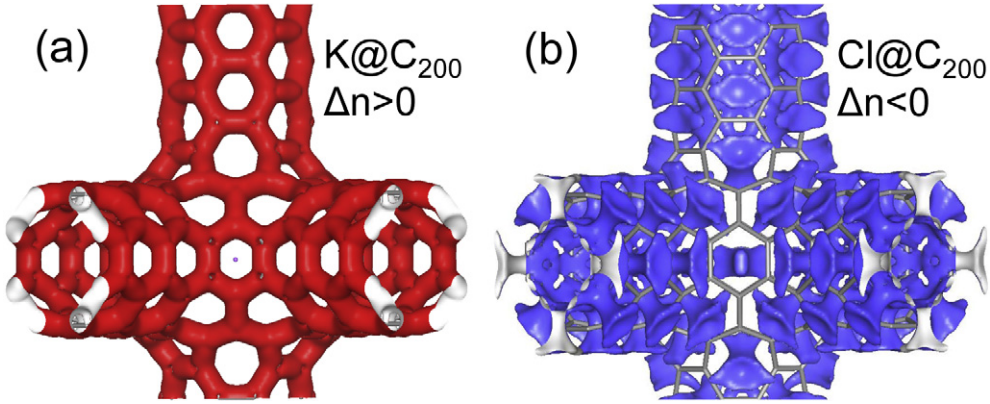

Figure 5. Electron density difference $\Delta n(\mathrm{A@C_{200}}) = n_{\mathrm{tot}}(\mathrm{A@C_{200}}) - n_{\mathrm{tot}}(\mathrm{A}) - n_{\mathrm{tot}}(\mathrm{C_{200}})$, providing insight into the charge flow in the C_{200} schwarzite following intercalation with A = K, Cl atoms. (a) $\Delta n(\mathrm{K@C_{200}})$ at the isodensity value $+0.04$ Å^{-3}. (b) $\Delta n(\mathrm{Cl@C_{200}})$ at the isodensity value -0.04 Å^{-3}.

Assuming, furthermore, the same average interlayer distance as in a graphene bilayer, we estimate the capacitance of the C_{400} schwarzite to be 34.3 F cm^{-3} material.

As an independent way to estimate the capacitance of the C_{400} schwarzite, we carefully inspected the total energy differences between neutral C_{200} and C_{400} systems, as well as the total energies of K@C_{200}, Cl@C_{200} and C_{400} containing both K and Cl. The latter structure, which contains one positively and one negatively charged C_{200} minimal surface per unit cell, is a superposition of K@C_{200} and Cl@C_{200}. The stabilizing interaction between the charged C_{200} substructures of 15.735 eV is partly due to the chemical interaction between the two electrodes, which we estimated to be 15.464 eV per unit cell in the pristine system. We assign the remaining part of the interaction energy, 0.271 eV, to be the energy associated with the electric field between the capacitor plates. To understand the meaning of this energy gain, we consider two parallel-plate electrodes carrying constant charges $+Q$ and $-Q$, approaching from infinity to form a parallel-plate capacitor of capacitance C, thereby gaining the energy $\Delta U = Q^2/(2C)$. Considering $\Delta U = 0.271$ eV and $|Q| = 0.42e$, the smaller of the charges transferred between the intercalant atoms and the neighboring electrodes, we can estimate the capacitance C per unit cell and the corresponding value in the bulk C_{400} schwarzite material, which turns out to be 12.6 F cm^{-3}.

We would like to point out that the above capacitance values are based on rough approximations and thus should be considered as order-of-magnitude estimates. Still, we are pleased that our estimate based on total energy differences in the intercalated system lies close to the estimate based on area and inter-plate distance. In any case, the estimated capacitance exceeds that of present day capacitors by several orders of magnitude. Should a material close to the postulated C_{400} schwarzite ever be synthesized, we must also consider the need to connect the two interpenetrating sublattices to two leads, which will be a nontrivial task. We also need to point out that the close proximity of the two electrodes in the schwarzite material promotes tunneling, which would eventually discharge the electrodes over time. Still, the expected capacitance of tens of farads per cubic centimeter is an appealing prospect.

In summary, we studied the stability, elastic properties and electronic structure of sp^2 carbon periodic minimal surfaces with negative Gaussian curvature, called schwarzites, using *ab initio* density functional calculations. Our studies of two primitive minimal surfaces, spanned by an underlying simple cubic lattice with 152 and 200 carbon atoms, indicate that these systems are very stable, rigid, and electrically conductive. The porous schwarzite structure allows for efficient and reversible doping by intercalation of electron donors or acceptors. We identified systems that should act as arrays of interconnected spin quantum dots or, when doped, exhibit ferromagnetic behavior. We also introduce two interpenetrating schwarzite structures as an unusual system that may find its use as the ultimate super-capacitor.

Acknowledgments

We thank Jeung Sun Ahn for useful comments and acknowledge the contributions of Thomas Moore and Daniel Enderich to the visualization of the schwarzite structures. DT was supported by the International Scholar fellowship at Kyung Hee University and funded by the National Science Foundation under NSF-NSEC grant 425826 and NSF-NIRT grant ECS-0506309. YK was supported by the NRF of Korea grant KRF-2009-0074951.

References

[1] Kroto H W, Heath J R, O'Brien S C, Curl R F and Smalley R E 1985 *Nature* **318** 162–3
[2] Dresselhaus M S, Dresselhaus G and Eklund P C 1996 *Science of Fullerenes and Carbon Nanotubes* (San Diego, CA: Academic)
[3] Jorio A, Dresselhaus M S and Dresselhaus G (ed) 2008 *Carbon Nanotubes: Advanced Topics in the Synthesis, Structure, Properties and Applications* (*Topics in Applied Physics* vol 111) (Berlin: Springer)
[4] Mackay A L 1985 *Nature* **314** 604–6
[5] Blinc R, Arcon D, Umek P, Apih T, Milia F and Rode A V 2007 *Phys. Status Solidi* b **244** 4308–10

[6] Petersen T, Yarovsky I, Snook I, McCulloch D G and Opletal G 2004 *Carbon* **42** 2457–69
[7] Wang Z X, Yu L P, Zhang W, Han J G, Zhu Z Y, He G W, Chen Y and Hu G 2003 *Chem. Phys. Lett.* **380** 78–83
[8] Merz K M, Hoffmann R and Balaban A T 1987 *J. Am. Chem. Soc.* **109** 6742–51
[9] O'Keeffe M, Adams G B and Sankey O F 1992 *Phys. Rev. Lett.* **68** 2325–8
[10] Kusner R B, Lahti P M and Lillya C P 1995 *Chem. Phys. Lett.* **241** 522–7
[11] Huang M-Z, Ching W Y and Lenosky T 1993 *Phys. Rev.* B **47** 1593–606
[12] Gaito S, Colombo L and Benedek G 1998 *Europhys. Lett.* **44** 525–30
[13] Vanderbilt D and Tersoff J 1992 *Phys. Rev. Lett.* **68** 511–3
[14] Mackay A L and Terrones H 1991 *Nature* **352** 762
[15] Phillips R, Drabold D A, Lenosky T, Adams G B and Sankey O F 1992 *Phys. Rev.* B **46** 1941–3
[16] Lenosky T, Gonze X, Teter M and Elser V 1992 *Nature* **355** 333–5
[17] Margine E R, Kolmogorov A N, Stojkovic D, Sofo J O and Crespi V H 2007 *Phys. Rev.* B **76** 115436
[18] Terrones H and Terrones M 1998 *Carbon* **36** 725–30
[19] Ceperley D M and Alder B J 1980 *Phys. Rev. Lett.* **45** 566
[20] Perdew J P and Zunger A 1981 *Phys. Rev.* B **23** 5048
[21] Troullier N and Martins J L 1991 *Phys. Rev.* B **43** 1993
[22] Kleinman L and Bylander D M 1982 *Phys. Rev. Lett.* **48** 1425
[23] Sánchez-Portal D, Ordejón P, Artacho E and Soler J M 1997 *Int. J. Quantum Chem.* **65** 453
[24] Soler J M, Artacho E, Gale J D, García A, Junquera J, Ordejón P and Sánchez-Portal D 2002 *J. Phys.: Condens. Matter* **14** 2745–79
[25] Hestenes M R and Stiefel E 1952 *J. Res. Natl Bur. Stand.* **49** 409–36
[26] Kittel C 2005 *Introduction to Solid State Physics* 8th edn (New York: Wiley)
[27] Dresselhaus M S and Dresselhaus G 2002 *Adv. Phys.* **51** 1–186
[28] Yoon M, Yang S, Hicke C, Wang E, Geohegan D and Zhang Z 2008 *Phys. Rev. Lett.* **100** 206806